Soft Matter

Cite this: *Soft Matter*, 2012, **8**, 399

www.rsc.org/softmatter

PAPER

Resonant properties of sessile droplets; contact angle dependence of the resonant frequency and width in glycerol/water mixtures

James S. Sharp*

Received 7th October 2011, Accepted 16th October 2011
DOI: 10.1039/c1sm06916k

A simple optical deflection technique was used to monitor the vibrations of small (microlitre) sessile droplets of glycerol/water mixtures when a puff of air was used to apply an impulse to the drops. A photodiode was used to detect time dependent variations in the intensity of laser light that was reflected from the droplets. The intensity variations obtained from droplets with masses in the range 0.0005–0.03 g were Fourier transformed to obtain information about the resonant properties (frequency and width of the resonance). These experiments were performed on a range of different substrates where the three phase contact angle formed by the droplets varied between 38 ± 2° and 160 ± 4°. This was repeated for droplets with glycerol compositions ranging from 10% to 75%. The measured resonant frequency values were found to be in good agreement with a recently developed 1-D theory of vibrations in sessile droplets which considers standing wave states around the meridonal profile length of the droplet. The widths of the resonances were also compared with modified theories which predict the influence of substrate effects, surface contamination effects and bulk viscous effects on the damping of capillary waves at the free surface of the droplets. These experiments indicate that the dominant source of damping in sessile liquid droplet is due to bulk viscous effects but that for small contact angles damping due to the droplet/substrate interaction becomes more important.

1 Introduction

Simultaneous measurements of viscosity and surface tension are challenging, particularly when the available volumes of the test liquid are small. One method by which researchers have tried to extract these quantities involves vibrating small liquid droplets. The resonant frequency and width of the various vibrational modes can then in principle be used to extract information about the stiffness (spring constant) of the droplets and the damping of their motion. The spring constant of the droplets is simply related to the surface tension[1–5] and the damping provides information about the viscosity of the liquid.[3,6]

The theory of vibrations in levitated droplets was originally developed by Lord Rayleigh[7] and was later extended by Chandrasekhar to include the effects of viscous damping.[8] More recently, Strani and Sabetta[9] and Smithwick and coworkers[10] derived a theory to describe the resonant frequencies of sessile droplets confined to a spherical bowl where the support angle could effectively be used to vary the contact angle on the surface. Although this theory was successfully extended to planar surfaces, determination of the contact angle dependent eigenvalues associated with the different vibrational modes of the droplet involved solving the determinant of an infinitely large matrix, limiting its use in any practical applications. A more recently developed model proposed by Noblin *et al.* offers a more intuitive interpretation of the origin of the vibrational modes of sessile droplets.[11] This theory considers the number of half integer wavelengths that can fit around the meridian profile length of a droplet and combines this information with the dispersion relation for capillary waves in an infinitely deep liquid bath to obtain an approximation for the frequencies of the resonant vibrational modes.

Although the theory of levitated droplets has been used to extract the viscosity from measurements of the damping in these systems,[5] very little work has been done to understand how the viscosity and contact angle influence damping in sessile droplets. Vukasonic and coworkers[12] give a detailed discussion of factors such as bulk viscous dissipation, boundary layer effects, surface contamination and moving contact line effects that influence the motion of Faraday waves on the surface of vibrated sessile droplets. However, a detailed mathematical treatment of the effects was not attempted. A number of other authors have also derived theories of damping in vibrated sessile and pendant droplets[4,13–15] but to the best of our knowledge no detailed theoretical studies have been performed on the contact angle dependence of energy dissipation mechanisms in supported drops which consider all these possible damping mechanisms.

School of Physics and Astronomy and Nottingham Nanotechnology and Nanoscience Centre, University of Nottingham, Nottingham, UK. E-mail: james.sharp@nottingham.ac.uk; Fax: +44 (0)115 9515180; Tel: +44 (0)115 9515142

A significant amount of experimental work on vibrating droplets has involved the study of free spherical droplets that are levitated using acoustic[16] or electromagnetic methods (see for example[1–3,5]). The original research in this area was largely motivated by studies of the effect of vibration on the formation of high purity crystals under zero gravity conditions.[4,9,10] However, the vibration of droplets also occurs during important industrial processes such as spray cooling and coating, inkjet printing, droplet atomisation and fuel injection.[12] Other applications include the use of isolated vibrating droplets during electric field enhanced liquid–liquid extraction,[4] electrospray synthesis of mixed oxide ceramics and for the measurement of surface tension[1–5] and equilibrium contact angle values[11,17,18] in simple liquids, liquid metals, alloys and in biological systems. Mchale and coworkers[19] have also recently studied vibrations in electrically driven 'liquid marbles' with large contact angles in an attempt to use them as analogues of free/levitated drops. Vibrating droplets have also been used to drive the internal mixing of multi-component systems.[20]

Experimental studies have been performed using either horizontally[21–23] or vertically[11,14] vibrated sessile droplets. The main approach to exciting vibrations in these droplets was to use a loudspeaker or surface acoustic wave generator[17] that was attached to the substrate on which the droplets were deposited. An alternative method of driving the oscillations in droplets involves the use of ac electric fields[18,19] in so called electrowetting experiments. This method facilitates control of the wetting interactions of small droplets by changing their interfacial energies *via* the introduction of surface charges while also enabling measurements of the resonant properties of small conducting liquid or 'leaky' dielectric drops to be performed. Methods of detecting the motion of droplets during vibration have involved the use of high speed image acquisition,[11,21,23] optical deflection based techniques (where a laser beam is passed through the droplet and its motion monitored using a position sensitive detector)[14,17] and optical tweezer based approaches.[24]

Recent experiments have also looked at the possibility of using droplet vibration to actuate the motion of small droplets on gradient energy surfaces[21,23,25,26] where a gradient in wettability caused by variations in chemical or topographical structure is used to direct their motion. This particular application appears to have generated renewed interest in the field of vibrating droplets and has resulted in a number of recent studies on the resonant behaviour of small liquid droplets on vibrated surface[4,11,13,17,21,22] and in electrically driven sessile droplets.[19,24] In many of the systems mentioned above, the presence of a solid substrate can play a key role in determining the resonant properties of the droplets. For example, the presence of the solid boundary could introduce additional frictional interactions in a sessile drop that are not experienced by levitated droplets. This type of frictional interaction would be expected to modify the amount of damping experienced by waves on the surface of the droplet. Such an interaction would be determined by the area of the drop in contact with the substrate and as such would be expected to vary with the drop size (mass) and the three phase contact angle subtended by the droplet at the substrate. Many of the studies described above were limited by the fact that they were performed over a limited range of contact angles and in many cases only a single surface/contact angle value was studied. This means that a detailed study of the contact angle dependence of the resonant properties (and damping effects in particular) has yet to be performed.

This paper describes a study of the contact angle dependence of both the resonant frequencies and widths of the lowest vibrational mode of sessile droplets containing mixtures of glycerol and water. The novelty in this study lies in the measurement and interpretation of the widths of the resonances of sessile droplets over a broad range of contact angles (~38–160°) and in the application of modified versions of detailed theories of energy dissipation/damping in liquid baths in determining these widths. We show that the resonant frequency of the droplets is accurately described by a recently developed 1-D theory of vibration in sessile droplets[11,27] and that the contact angle and viscosity dependence of the widths of the resonant peaks are consistent with the predictions of the magnitudes of damping factors obtained from theory. We also show that for large contact angles, the magnitude of damping effects in the droplets is consistent with bulk viscous dissipation of energy, but that for contact angles less than ~70° the influence of the substrate becomes more important. To the best of our knowledge, this is the first detailed study of the combined contact angle and viscosity dependence of damping effects in sessile liquid droplets and their influence upon the widths of droplet resonances.

2 Experimental section

Microlitre droplets containing mixtures of glycerol and water with masses in the range 0.005–0.03g were placed on different substrates using an adjustable microlitre pipette. Pure glycerol (Sigma UK, Gillingham) was used as received and distilled deionised water was obtained from an Elga water purification system. Glycerol/water solutions with compositions in the range 10–75% were made by mixing the pure liquids together by mass. The substrates used included single crystal silicon wafers (Si, [100] orientation, native oxide intact), spin-cast polymer films (Polystyrene (PS, 600 kDa) and Polymethylmethacrylate (PMMA, 600 kDa), both obtained from Polymer Source, Quebec) deposited from solutions in toluene, Polydimethylsiloxane (PDMS, Sylgard 182) and a fine grade of hydrophobic sand sold as a child's toy (trade name "Aquasand"). All of these substrates were prepared as described previously.[27]

Small droplets were placed on the substrates and then weighed using a digital balance. The mass of each droplet was determined to within ±0.0001g. Several small puffs of air were then applied to the droplets by quickly blowing on the droplet quite hard and by mouth. This initial vibration was performed to enable the droplets to sample nearby configurations and to adopt a shape which corresponded to the equilibrium contact angle for each surface. Previous work has shown that vibrating the droplets overcomes contact line pinning effects and results in reproducible contact angles.[11,27,28] After this initial vibration, the shape of the droplets was inspected to ensure that the contact angles were the same when viewed from different directions.

The substrate and droplet were then mounted on an optical post and a laser beam (HeNe, 633 nm) was passed through the droplet, reflected off the substrate and allowed to fall on the surface of a low cost photodiode connected to a home-built

amplifier circuit (See insets Fig. 1). The diameter of the laser beam used was 0.8 mm and the droplet radii varied between 1mm and 4mm depending upon their mass and the contact angle. During data collection, an impulse was applied to each droplet by gently blowing on it from above. The application of the impulse made the free surface of the droplet vibrate and caused the position of the laser spot on the photodiode to vary with time. The time dependent intensity variations measured by the photodiode were recorded using a National Instruments USB Data acquisition card (USB-6008) and software written in Matlab (Mathworks). Data were collected over a period of 5 s using a sampling frequency of 1 kHz. The data was then Fourier transformed to obtain information about the vibrational frequencies of each droplet. The process of blowing on each droplet was repeated 3 times to ensure reproducibility and was performed on droplets with glycerol compositions ranging from 10% to 75%. In all cases, the contact line was observed to remain pinned while the free surface of the droplet vibrated and the resonant properties of the droplets were found to be the same within experimental error during each attempt. Fig. 1 shows examples of time dependent intensity data collected from small droplets of a 10% glycerol solution and a 75% glycerol solution supported on hydrophobic sand substrates. The corresponding Fourier transforms are also shown in this figure. In each case, the central position and the width (full width at half maximum) of the peak associated with the lowest vibrational mode were recorded. After each experiment the droplet and substrate were removed and reweighed to ensure that significant mass changes had not occurred. It was found that the mass of the droplet did not change within the limits of experimental uncertainty ($\pm 0.0001g$) during the course of the experiments. The glycerol solutions were also sealed in air tight containers when not being used to avoid problems associated with the hygroscopic nature of glycerol and the effects of contamination from the air. These precautions were found to be sufficient to ensure that significant changes in the composition of the droplets did not occur during the experiments.

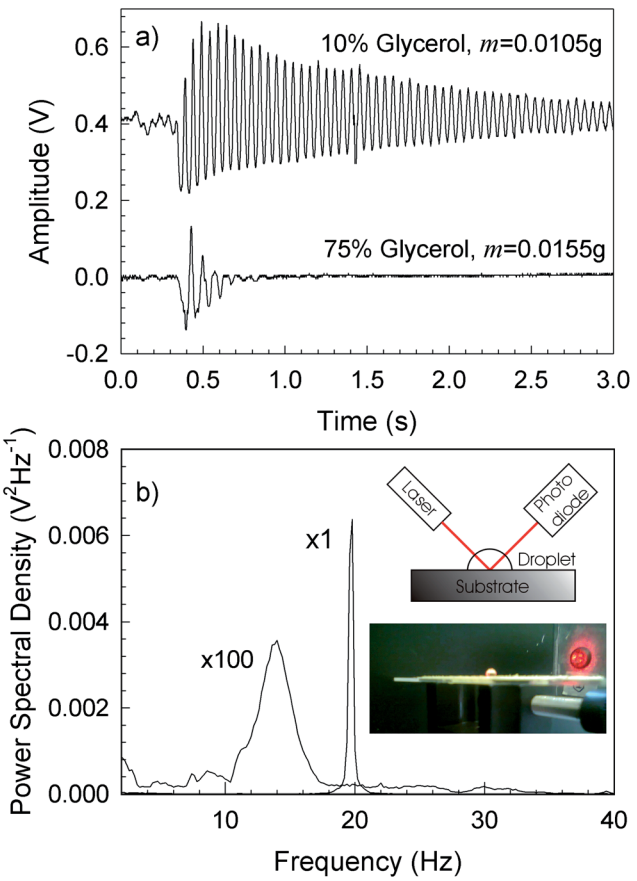

Fig. 1 Time and frequency dependence of the oscillations of microlitre glycerol/water droplets. The top panel (a) shows the time dependent intensity variations obtained for a 0.0105g droplet containing 10% glycerol (top) and a 0.0155g droplet containing 75% glycerol (bottom) supported on Aquasand substrates. The bottom panel (b) shows the power spectral density obtained by Fourier transforming the data in the top panel. The right hand peak corresponds to the resonant frequency of the 10% glycerol droplet and the left hand peak to that of the 75% glycerol droplet. The numbers at the side of the peak correspond to multiplicative scaling factors that were used to enable simultaneous viewing of the frequency response of the two droplets. The insets in panel (b) show a schematic diagram of the simple laser deflection method used to detect the droplet oscillations and a photograph of the experimental setup including a glycerol/water droplet on an Aquasand substrate. This photograph also shows the scattered laser beam striking the photodiode which appears as a bright red halo around the photodiode aperture.

Measurements of the contact angle (θ_m in degrees) were performed by collecting images of small sessile glycerol/water droplets using a webcam (as described previously[27]). The contact angle measured on a given substrate was found to be the same (within error) for all of the glycerol compositions studied. Fig. 2 shows examples of images similar to those that were used to extract the contact angle values on PDMS and Aquasand substrates. Table 1 gives a summary of the measured contact angles for all of the substrates studied.

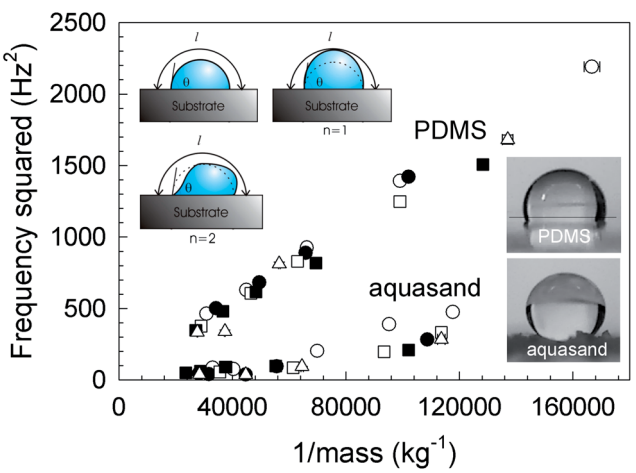

Fig. 2 Mass dependence of the resonant frequency of sessile glycerol/water droplets. The square of the resonant frequency (f^2) is plotted as a function of the inverse mass ($1/m$) for droplets supported on PDMS ($\theta = 118 \pm 3°$) and Aquasand ($\theta = 160 \pm 4°$) surfaces. Data are shown for droplets comprising 10% (○), 25% (●), 50% (□), 60% (■) and 75% (△) glycerol. The photographs shown as insets are similar to the ones that were used to measure the contact angles on these surfaces (see text). The diagrams shown in the top left show a droplet at rest and the shapes of the $n = 1$ and $n = 2$ sessile droplet modes respectively.

Table 1 Measured contact angle values for the substrates used in this study. The contact angle value measured on each substrate was found to be the same (within experimental uncertainty) for all of the glycerol compositions studied

Substrate	Contact Angle (degrees)
Silicon	38 ± 2
PMMA	71 ± 2
PS	91 ± 2
PDMS	118 ± 3
Aquasand	160 ± 4

3 Results and discussion

Glycerol/water mixtures are an excellent system for studying the separate influences of surface tension and viscosity upon the resonant response of small sessile liquid droplets. Pure water and glycerol have similar surface tension values of ~72 mJm^{-2} and ~63 mJm^{-2} [29] respectively. However, the viscosities of water and glycerol differ by over three orders of magnitude.[30,31] The fact that these liquids are miscible in all proportions means that the viscosity of mixtures of the two can be systematically varied over the range 0.001–1 Pas while keeping the surface tension approximately constant. The effects of the increase in viscosity of glycerol/water mixtures with higher glycerol composition can be seen clearly in Fig. 1. The time dependent intensity oscillations obtained from the droplet comprising 10% glycerol persist for over 3 s while the oscillations of the more viscous 75% glycerol droplet are rapidly damped. This increase in damping is a characteristic of increased viscous dissipation of energy within the droplets and is reflected in the Fourier transform by a broadening of the resonance peak at higher glycerol compositions.

3.1 Resonant frequency of sessile droplets

The resonant frequency of sessile liquid droplets can be calculated by using a theory that was originally developed by Noblin *et al.*[14] This model assumes that under conditions of resonant vibration, the profile length (l) of the droplet (see inset Fig. 2) will contain a half integer number of wavelengths (λ), such that

$$l = 2R\theta = \frac{n\lambda}{2} \tag{1}$$

where R is the radius of curvature of the droplet, θ is the three phase contact angle and n is an integer corresponding to the mode number ($n = 2,3,4\ldots$). In this and all subsequent equations, the angle θ is given in radians and is related to the measured contact angle (θ_m, measured in degrees) by the equation $\theta = \theta_m \frac{\pi}{180}$. Under the influence of small amplitude vibrations, such as those observed in the present experiments, the three phase contact line is assumed to remain fixed during vibration and as such is expected to coincide with the position of nodes in the excited waveform.

The volume, V, of a small droplet can be used to determine its radius of curvature if its shape is approximated to that of a spherical cap such that;

$$V = \frac{m}{\rho} = \frac{\pi R^3}{3}\left(\cos^3\theta - 3\cos\theta + 2\right) \tag{2}$$

where m is the mass of the droplet and ρ is its density.

The spherical cap approximation used in deriving the above equation is only valid when the radius of curvature is smaller than the capillary length,[27] *i.e.* when $R < L_{cap} = \left(\frac{\gamma}{\rho g}\right)^{1/2}$, where γ is the surface tension of the liquid and g is the acceleration due to gravity. In this regime, surface tension is expected to dominate over the influence of gravity which acts to flatten the profile of the droplet and to form a puddle. For pure water $L_{cap} \sim 2.7mm$, for pure glycerol $L_{cap} \sim 2.3mm$ and for mixtures of glycerol and water the value of L_{cap} is expected to lie between these values. The use of eqn (2) shows that the spherical approximation is valid for contact angles larger than ~55° and ~60° in the case of pure water and pure glycerol respectively, over the range of droplet masses studied.

The dispersion properties of waves on the surface of the droplet can be approximated to those obtained for capillary waves on an infinitely deep liquid bath[32] providing that the average height of the droplet is larger than the characteristic length scale $\sim \frac{\lambda}{2\pi}$ associated with the surface waves. Doing this gives an expression for the frequency, f, of the form[32]

$$f = \alpha\left(\frac{2\pi\gamma}{\rho\lambda^3}\right)^{\frac{1}{2}} \tag{3}$$

where α is a constant of order unity which accounts for the simplifying assumptions made in the application of the above formula to droplets of a finite size and to the fact that the theory of the droplets considered here uses a simplified one dimensional approach.

Combining eqn (1), (2) and (3) gives an expression for the contact angle dependence of the frequencies of the vibrational modes of sessile droplets.[27]

$$f_n = \frac{\alpha\pi}{2}\left(\frac{n^3\gamma}{24m}\frac{(\cos^3\theta - 3\cos\theta + 2)}{\theta^3}\right)^{\frac{1}{2}} \tag{4}$$

This has a similar functional form to the vibration frequencies obtained for free/levitated droplets.[8,19]

$$f_j = \left(\frac{j(j-1)(j+2)\gamma}{3\pi m}\right)^{\frac{1}{2}} \tag{5}$$

where $j = 2,3,4\ldots$ is the mode number.

Sharp *et al.*[27] considered the validity of the infinite bath approximation used in deriving eqn (4) and found that it works best in the limits of high contact angles and for mode numbers larger than $n = 2$. However, these same authors performed detailed measurements of the contact angle dependence of the resonant frequency of sessile water droplets and found that eqn (4) worked well and that values of $\alpha \sim 0.81$ and $n = 2$ could be used to accurately predict the frequencies of the lowest vibrational mode in sessile droplets with contact angles in the range 12–160°.

Eqn (4) predicts a linear scaling between the square of the resonant frequency and the reciprocal of the droplet mass. Fig. 2

shows examples of plots of f^2 *vs.* $1/m$ for sessile glycerol/water droplets with different compositions on two of the surfaces studied (PDMS and Aquasand). The linear relationship between f^2 and $1/m$ seems to hold for these two surfaces for all of the droplet compositions studied with perhaps some evidence of deviation from linearity in the Aquasand data for the largest mass values reported. Moreover, the slopes of these plots on a given surface are insensitive to the composition of the droplets. This is to be expected based upon the fact that the surface tension does not vary significantly with increasing glycerol composition and also that the measured contact angle, θ_m, was found to be the same within error for each of the droplet compositions on a given substrate.

Fig. 3 shows a summary of all the resonant frequency data obtained for the lowest mode of vibration for the sessile drops studied. This plot shows how the slope of f^2 *vs.* $1/m$ changes as a function of contact angle for each of the droplet compositions. The dashed and solid lines show the predictions of eqn (4) for the contact angle dependence of the resonant frequency that were calculated using values of $\alpha = 0.81$, $n = 2$(after Sharp *et al.*[27]) and values of $\gamma = 72\text{mJm}^{-2}$ for pure water and $\gamma = 63\text{mJm}^{-2}$ for pure glycerol. The data and form of eqn (4) both display a non-monotonic dependence upon contact angle with a maximum at $\sim 70^\circ$ which corresponds to the contact angle that gives the shortest meridonal profile length for a fixed droplet mass.[27] The experimental data in Fig. 3 are in good agreement with the predictions of the simple theory derived above. This shows that the surface tension values for glycerol and water determine the appropriate scale for the stiffness/spring constant of the droplets studied. The justification for using $n = 2$ to describe the lowest frequency vibrational mode arises from the fact that this is the lowest mode which satisfies the incompressibility condition implied by setting $V = \frac{m}{\rho}$ in eqn (2). The $n = 1$ mode corresponds to the case where only one half of a wavelength fits along the meridonal length of the droplet and necessarily requires a change in volume if the contact line remains pinned (see inset in Fig. 2). Such a change in volume is forbidden for an incompressible fluid. However, the $n = 2$ mode enables motion of the fluid along the drop profile while still being able to conserve volume. In the limit of large amplitude vibrations the contact line is more likely to move and the above restriction is likely to be relaxed. Under these conditions it should be possible for antinodes to exist at the contact line[14] and in the case of the $n = 1$ mode, a single node would appear at the top of the droplet. In this case, both motion of fluid within the droplet and volume conservation should be possible and the $n = 1$ mode should appear in the frequency response of the droplet. The fact that the lowest frequency mode observed in the present set of experiments is best described by setting $n = 2$ for all contact angles confirms that the contact line remained pinned during the low amplitude vibrations that were applied to the droplets.

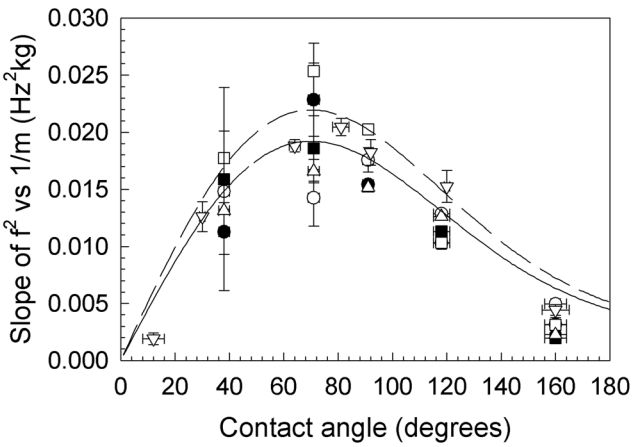

Fig. 3 Contact angle dependence of the resonant frequency of sessile glycerol/water droplets. Data are shown for the slope of f^2 *vs.* $1/m$ as a function of the contact angle for droplets comprising 10% (○), 25% (●), 50% (□), 60% (■) and 75% (△) glycerol. These data were obtained from plots similar to those shown in Fig. 2. The dashed line shows the prediction of eqn (4) that was calculated using the surface tension of water ($\gamma = 72\text{mJm}^{-2}$) and the solid line shows the prediction of this equation calculated for pure glycerol ($\gamma = 63\text{mJm}^{-2}$, see text).

3.2 Damping in sessile droplets

Damping of the motion of sessile droplets is manifested as an exponential decay of the amplitude of vibration similar to that observed in Fig. 1. The amplitude, A, of the time dependent intensity variations shown in Fig. 1 can be written in the form $A = A_o \exp(-\Gamma(t - t_o))\cos(2\pi ft + \phi)$, where t is the time, ϕ is a phase factor and A_o is the amplitude immediately after the impulse was applied (at time $t = t_o$). The decay constant associated with the exponential decay of the amplitude of the intensity signal, Γ, is simply equal to the full width at half maximum of the resonant peak in the Fourier transforms (power spectra) of the time dependent data. Previous studies of the vibration of levitated droplets have confirmed that the damping constant scales as $\Gamma \sim \frac{\eta}{m^{2/3}\rho^{1/3}}$.[5,8] According to this expression, the width of the resonant peak should increase with increasing viscosity (η) for levitated droplets. Such an increase in width is also observed in the data shown in the bottom panel of Fig. 1 for sessile droplets.

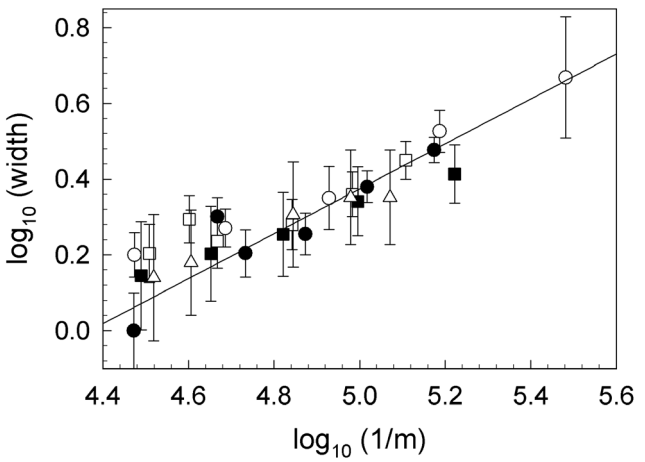

Fig. 4 Log-log plot of the peak width as a function of $1/m$ for 10% glycerol droplets supported on different substrates. The plot shows data for sessile droplets on Si (○, $\theta = 38 \pm 2$), PMMA (●, $\theta = 71 \pm 2$), PS (□, $\theta = 91 \pm 2$), PDMS (■, $\theta = 118 \pm 3$) and Aquasand (Δ, $\theta = 160 \pm 4$) substrates. Data points have been shifted to allow comparison of the slopes of the curves. The solid line shows the average slope obtained from the fit to the data. This line has a slope of 0.6 ± 0.1.

The top panel in Fig. 4 shows a log-log plot of the width of the resonant peaks as a function of $1/m$ obtained for 10% glycerol solutions on substrates with different contact angle values. In this plot the vertical position of the curves has been shifted so that the slopes of the experimental data can be compared. The slope of the solid line corresponds to the average slope of all the data points shown and gives the power law dependence of the width (Γ) of the resonant peak on the inverse mass ($1/m$). The gradient of this line was found to have a value of 0.6 ± 0.1 which compares favourably with the $2/3 = 0.67$ inverse mass power law dependence of the width of the resonance in levitated droplets.

The case of damping in sessile droplets may be complicated by the fact that Γ is likely to be dependent upon the contact angle in a non-trivial way. There are a number of possible damping mechanisms that may exist in sessile droplets relating to the presence of a solid boundary and three phase contact line which do not occur for free or levitated droplets. It is noteworthy that the range of values encompassed by the fit to the slope of the data in the top panel of Fig. 4 is quite broad (0.5–0.7). Such a large variation in the inverse mass power law dependence with changing contact angle may be indicative of the presence of these additional damping mechanisms. This broad range of values may also suggest that the mass power law dependence of damping effects varies with the contact angle.

Determining the relative influences of bulk and interfacial damping mechanisms requires a knowledge of both the magnitudes of the measured widths that would be expected for each type of mechanism and also their contact angle and mass (droplet size) power law dependencies. In the following sections the expected contact angle dependence of damping effects due to bulk viscous dissipation, solid boundary layer effects and contaminated liquid surfaces are considered. Other authors have also considered the effects of damping due to a moving contact line.[12,33–35] However, the observations and discussion presented above rule out the possibility of a moving contact line in these experiments. The interested reader is directed to the studies of Christiansen *et al.*[33] and Milner[36] for a detailed discussion of these effects.

3.2.1 Bulk viscous damping. A number of authors have considered bulk viscous damping[12,32,33] and have derived an expression for the damping coefficient, Γ_{bulk}, such that

$$\Gamma_{bulk} = \frac{2\eta}{\rho}k^2 = \frac{2\eta}{\rho^{1/3}}\left(\frac{4\pi^2 f^2}{\gamma}\right)^{2/3} \quad (6)$$

where $k = \frac{2\pi}{\lambda}$ is the wavenumber associated with the surface waves. In the above equation we have assumed that the dispersion relation given by eqn (3) can be used to relate the frequency of vibration to the wavenumber of the surface waves. Inserting the expression for the resonant frequency of the n^{th} vibrational mode given by eqn (4) gives an expression for the bulk viscous damping coefficient.

$$\Gamma_{bulk} = \frac{\eta}{\rho^{1/3}}\frac{n^2\alpha^{4/3}\pi^{8/3}}{2}\left(\frac{\cos^3\theta - 3\cos\theta + 2}{3m\theta^3}\right)^{2/3} \quad (7)$$

As for the case of damping in free/levitated droplets the bulk viscous damping coefficient scales with $\sim \frac{\eta}{m^{2/3}\rho^{1/3}}$, but there is an additional geometric factor which takes into account the contact angle dependence.

3.2.2 Boundary layer damping. The presence of a solid boundary or substrate will also influence the damping of capillary waves on the surface of the drop. The role of solid boundaries in influencing the damping of Faraday waves in containers of finite size has been considered in detail by Milner.[36] The assumption of a no-slip boundary condition at a solid interface means that the fluid velocity must fall from a finite value to zero within some small distance, $\delta = \left(\frac{\eta}{\pi\rho f}\right)^{1/2}$, of the solid boundary. The decay of the velocity over such short distances results in the introduction of steep velocity gradients which give rise to a non-negligible amount of energy dissipation in the fluid.[33,36] Milner[36] specifically dealt with the case of damping of Faraday waves on the planar surface of an infinitely deep liquid bath of finite width, L. The boundary layer was defined to be within a distance, δ, of the edges of the bath. The resulting damping factor was shown by Milner to be given by the expression

$$\Gamma_{wall} = \frac{2\pi f\delta}{L} = \frac{2}{L}\left(\frac{\pi f\eta}{\rho}\right)^{1/2} \quad (8)$$

Caution should be exercised in applying the above model to the case of a compact droplet with a curved surface.[12] However, the above formula enables estimates of the mass power law dependencies and magnitudes of the resonant widths expected for boundary layer damping in sessile droplets to be obtained. These effects are expected to be largest in the region close to the three phase contact line where the gradients in velocity are the steepest.[12] In deriving the relevant expression for the damping factor, the size of the bath is approximated to the length of the meridonal profile of the droplet such that $L = 2R\theta$. Combining this result with eqn (8) and expressions for the radius of curvature and resonant frequency of the droplets given by eqn (2) and (4) respectively, gives an expression for the damping coefficient due to solid boundary effects of the form

$$\Gamma_{wall} = \left(\frac{n}{2}\right)^{3/4}\pi^{4/3}\gamma^{1/4}\left(\frac{\alpha\eta}{2\rho^{1/3}}\right)^{1/2}\left(\frac{\cos^3\theta - 3\cos\theta + 2}{3m\theta^3}\right)^{7/12} \quad (9)$$

3.2.3 Contaminated surface layer. A further source of damping could originate from contamination of the droplet's free surface. The presence of such a layer would not only influence the damping of the droplet but also the surface tension and might be partly responsible for the reduction in resonant frequency which was parameterised by the constant α in eqn (4). Milner[36] and Miles[34] derived expressions for the damping coefficient due to a contaminated surface layer and showed that the maximum damping coefficient was given by the form

$$\Gamma_{surf} = 2\pi\delta fk \quad (10)$$

Inserting the expressions for the dispersion relation for capillary waves and the resonant frequency of the droplet given by eqn (3) and (4) respectively, the damping coefficient due to surface contamination effects takes the form

$$\Gamma_{surf} = \alpha^{7/6}\pi^{7/3}\gamma^{1/4}\left(\frac{n}{2}\right)^{7/4}\left(\frac{2\eta}{\rho^{1/3}}\right)^{1/2}\left(\frac{\cos^3\theta - 3\cos\theta + 2}{3m\theta^3}\right)^{7/12} \quad (11)$$

As in the case of the boundary layer damping described above, this expression is based upon a theory that was developed for Faraday waves on planar surfaces. It is noteworthy that the functional form of the above equation is similar to that expected for solid boundary effects, but that the damping due to surface contamination is larger than that due to boundary layer damping by a factor of $n\alpha^{2/3}\pi(\sim 5.5$ for the $n = 2$ mode with $\alpha = 0.81$) for all contact angles.

3.2.4 Dominant source of damping in sessile droplets. To identify the dominant source of damping during the vibration of sessile drops it is instructive to consider the functional forms given by eqn (7), (9) and (11). Eqn (7) predicts that the bulk damping coefficient (and hence the full width measured half maximum of the resonant peak) should scale with $1/m^{2/3}$ while the other two equations indicate that interfacial effects should scale with $1/m^{7/12}$. In principle it should be possible to determine the dominant damping mechanisms based upon the mass power law dependence of the width of the resonances. However, $7/12 \sim 2/3$ and both of these power law dependencies are encompassed by the range of values obtained from the fit to the data shown in Fig. 4. As discussed above, the broad range of values encompassed by the uncertainties in the slope of this plot may be indicative of the fact that the relative contributions of bulk and surface effects depends upon the contact angle. Fig. 5 shows that both $1/m^{2/3}$ and $1/m^{7/12}$ power law dependencies can be used to fit the width data within the limits of experimental uncertainty. As such, a simple analysis of the mass power law dependence of the resonant widths is not sufficient to determine the dominant damping mechanism in sessile droplets over the range of masses studied.

Closer inspection of eqns (7), (9) and (11) shows that the magnitude of the damping factors predicted for bulk and interfacial effects are expected scale differently with the viscosity and density of the fluid. Bulk effects are expected to scale as $\frac{\eta}{\rho^{1/3}}$ while interfacial damping gives a $\frac{\eta^{1/2}}{\rho^{1/6}}$ dependence. A comparison of the scaling of the experimentally determined widths with the ratio $\frac{\eta}{\rho^{1/3}}$ should therefore provide some indication of the dominant damping mechanism for each of the contact angles and compositions studied.

Fig. 6 shows the slope of the peak width *vs.* $1/m^{2/3}$ (top panel) as a function of $\frac{\eta}{\rho^{1/3}}$ for all the compositions studied. The values of the viscosity and density used for the different glycerol water compositions in this plot were obtained from ref. 30 and 31. This plot shows that the slope of the peak width *vs.* $1/m^{2/3}$ scales linearly with the ratio $\frac{\eta}{\rho^{1/3}}$ for all but the lowest contact angle studied. According to the equations derived above, this is a signature of bulk dissipation effects dominating the damping behaviour of the droplets. Moreover, if values of the viscosity and density obtained from bulk solutions (see refs. 30 and 31)

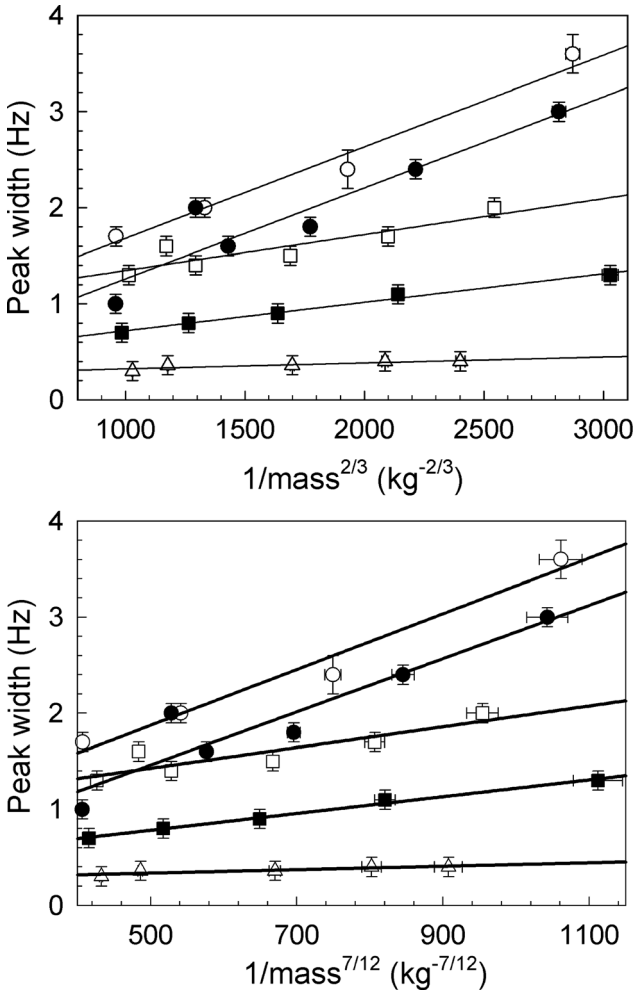

Fig. 5 Measured peak width for 10% glycerol droplets supported on different substrates. The top panel shows plots of the full width of the resonant peak (at half maximum) *vs.* $(1/m)^{2/3}$ for sessile droplets on Si (○, $\theta = 38 \pm 2$), PMMA (●, $\theta = 71 \pm 2$), PS (□, $\theta = 91 \pm 2$), PDMS (■, $\theta = 118 \pm 3$) and Aquasand (Δ, $\theta = 160 \pm 4$) substrates. The bottom panel shows the measured width data on these substrates plotted as a function of $(1/m)^{7/12}$. The solid lines are straight line fits to the data.

along with values of $\alpha = 0.81$ and $n = 2$ are used, the values predicted for the measured widths agree with the predictions of eqn (7) to within a factor of ~2–3 for all compositions studied over this range of contact angles.

The data collected from the surface with the smallest contact angle (Si), clearly has a weaker dependence upon the ratio $\frac{\eta}{\rho^{1/3}}$, than the data obtained for surfaces with larger contact angles and cannot be described using a linear fit. There is also some evidence of curvature in the data obtained for the PMMA surface ($\theta = 71°$), although these data can still be adequately described using a linear fit within the limits of experimental uncertainty. The weaker dependence of the slope at lower contact angles may be indicative of interfacial damping effects in the droplets. Eqn (9) and (11) predict that damping due to interfacial effects should scale as $\frac{\eta^{1/2}}{\rho^{1/6}}$ and also as $1/m^{7/12}$. The bottom panel in Fig. 6 shows a plot of the slope of the width *vs.* $1/m^{7/12}$ as a function of $\frac{\eta^{1/2}}{\rho^{1/6}}$ for

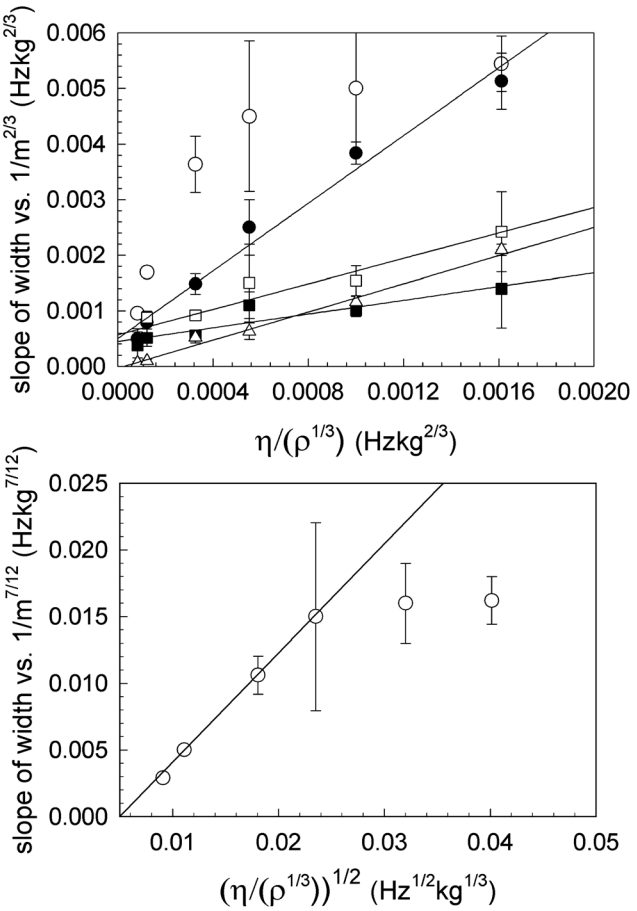

Fig. 6 Combined viscosity and density dependence of damping effects in sessile glycerol/water droplets. The top panel shows data for the slope of the full width at half maximum *vs.* $(1/m)^{2/3}$as a function of the ratio $\frac{\eta}{\rho^{1/3}}$ for sessile droplets on Si (○, $\theta = 38 \pm 2$), PMMA (•, $\theta = 71 \pm 2$), PS (□, $\theta = 91 \pm 2$), PDMS (■, $\theta = 118 \pm 3$) and Aquasand (Δ, $\theta = 160 \pm 4$) substrates. The bottom panel shows a plot of the slope of the width *vs.* $(1/m)^{7/12}$ as a function of $\frac{\eta^{1/2}}{\rho^{1/6}}$ for droplets on Si substrates. The solid lines in all of the plots are straight line fits to the data.

the data obtained from the Si surface. This plot shows that for values of the ratio $\frac{\eta^{1/2}}{\rho^{1/6}} \leq 0.0235$ (corresponding to concentrations less than 60% glycerol) the Si substrate data does show a linear dependence upon this quantity. This would seem to indicate that interfacial effects dominate the behaviour at contact angles ~38° for glycerol concentrations less than or equal to 60%. A greater influence of interfacial damping effects at lower contact angles is to be expected as more of the droplet volume is expected to fall within the regions corresponding to the free surface and substrate boundary layers.

For values of $\frac{\eta^{1/2}}{\rho^{1/6}}$ larger than 0.0235 (concentrations larger than 60%), the slopes shown in the bottom panel of Fig. 6 have a weaker dependence on $\frac{\eta^{1/2}}{\rho^{1/6}}$ and appear to level off as this parameter increases. The reason for this is not clear at this stage. One possible explanation could be the fact that the damping factors derived in eqn (9) and (11) also scale with $\gamma^{1/4}$. However, the surface tension of glycerol/water mixtures does not depend strongly upon composition.[29] Inclusion of a factor of $\gamma^{1/4}$ in the scaling shown in the plot in the bottom of Fig. 6 does not have a significant influence on the shape of the curve shown over the range of compositions studied.

If interfacial effects influence the damping for small contact angles, then it is instructive to consider whether damping is dominated by contaminated surface layer effects or by damping in a layer near the substrate. The effects of surface contamination cannot be ruled out entirely in these experiments, but the liquids that were used in these experiments were stored carefully to prevent contamination. This suggests that this mechanism is unlikely to be the dominant interfacial damping mechanism in the experiments described here. In addition, the fact that individual experiments typically took less than 1 min to perform and that the timescale associated with contamination of a clean air/water interface is ~5 min makes this damping mechanism less likely to be important.[12] Calculations based upon eqn (9) and (11) which use values of the surface tension, viscosity and density obtained from the literature[29–31] along with values of $\alpha = 0.81$ and $n = 2$ show that damping factors obtained for solid boundary layer effects agree with the measured widths to within a factor of 2 for the lowest contact angle studied. However, eqn (11) predicts that contaminated surfaces would result in widths that are a factor of ~10 larger than those measured here. All of the above factors seem to suggest that solid boundary layer damping is likely to be the dominant interfacial damping mechanism for the droplets studied here.

As stated above, the treatment of interfacial effects in this work is quite basic and the equations are based on expressions that were derived for waves on planar liquid surfaces on top of infinitely deep liquid baths. More detailed theories of damping at the solid/liquid and liquid/air interfaces need to be derived for compact sessile droplets where the droplet height and the radius of curvature of the droplet are finite. In addition to this, it is worth noting that the smallest contact angles (<55–60°) studied fall out of the range of validity of the spherical cap approximation used in eqn (2) when deriving the droplet volume and corresponding damping factors. However, despite the limitations of the theoretical approach used, the prediction of the resonant frequencies obtained from eqn (4) and the magnitudes of the width/damping factors predicted by eqn (7) and (9) are encouraging. The results of this study suggest that further refinement of the experimental techniques and the theoretical approach used may enable the surface tension and viscosity to be determined from single measurements of the resonant frequency and width values of sessile liquid droplets.

4 Conclusions

A simple optical detection method was used to monitor the vibrations of microlitre sessile droplets of glycerol/water mixtures on different substrates. Fourier transforms of the time dependent intensity data were used to extract the frequency and width of the resonant peak corresponding to the lowest frequency mode of vibration. The contact angle dependence of the resonant frequency was shown to be in good agreement with the predictions of a modified theory of droplet vibration which

considers standing wave states along the profile length of the droplets. The widths of the resonances for different droplet compositions were compared to theoretical predictions for the effects of damping due to bulk viscous dissipation, dissipation at the substrate interface and damping due to surface contamination. For contact angles larger than ~71° the width of the resonant peaks was found to be consistent (to within a factor of 2–3) with the presence of damping of the surface waves due to bulk viscous effects. For lower contact angles where more of the droplet volume was encompassed within the thickness of the solid/liquid boundary layer, damping due to the presence of substrate effects appear to influence energy dissipation within the droplets.

References

1 I. Egry, G. Lohoefer and G. Jacobs, *Phys. Rev. Lett.*, 1995, **75**(22), 4043–4046.
2 I. Egry, H. Giffard and S. Schneider, *Meas. Sci. Technol.*, 2005, **16**, 426–431.
3 W. Meier, G. Greune, A. Meyboom and K. P. Hofmann, *Eur. Biophys. J.*, 2000, **29**, 113–124.
4 E. D. Wilkes and O. A. Basaran, *Phys. Fluids*, 1997, **9**(6), 1512–1528.
5 R. J. A. Hill and L. Eaves, *Phys. Rev. E: Stat., Nonlinear, Soft Matter Phys.*, 2010, **81**, 056312.
6 I. Egry, G. Lohofer, I. Seyhan, S. Schneider and B. Feuerbacher, *Appl. Phys. Lett.*, 1998, **73**(4), 462–463.
7 R. W. S. Rayleigh, *Proc. R. Soc. London*, 1879, **29**, 71–97.
8 S. Chandrasekhar, *Proc. London Math. Soc.*, 1959, **3**(9), 141–149.
9 M. Strani and F. Sabetta, *J. Fluid Mech.*, 1984, **141**, 233–247.
10 R. W. SmithwickIII and J. A. M. Boulet, *J. Colloid Interface Sci.*, 1989, **130**, 588–596.
11 X. Noblin, A. Buguin and F. Brochard-Wyart, *Eur. Phys. J. Spec. Top.*, 2009, **166**, 7–10.
12 B. Vukasinovic, M. K. Smith and A. Glezer, *J. Fluid Mech.*, 2007, **587**, 395–423.
13 F. Celestini and R. Kofman, *Phys. Rev. E: Stat., Nonlinear, Soft Matter Phys.*, 2006, **73**, 041602.
14 X. Noblin, A. Buguin and F. Brochard-Wyart, *Eur. Phys. J. E*, 2004, **14**, 395–404.
15 M. Strani and F. Sabetta, *J. Fluid Mech.*, 1988, **189**, 397–421.
16 C. L. Shen, W. J. Xie and B. Wei, *Phys. Rev. E: Stat., Nonlinear, Soft Matter Phys.*, 2010, **81**, 046305.
17 S. Yamamkita, Y. Matsui and S. Shiokawa, *Jpn. J. Appl. Phys.*, 1999, **38**, 3127–3130.
18 Y. Karadag, A. Jonas, N. Tasaltin and A. Kiraz, *Appl. Phys. Lett.*, 2011, **98**, 194101.
19 G. McHale, S. J. Elliot, M. I. Newton, D. L. Herbertson and K. Esmer, *Langmuir*, 2009, **25**, 529–533.
20 F. Mugele, J. C. Baret and D. Steinhauser, *Appl. Phys. Lett.*, 2006, **88**, 204106.
21 S. Daniel, S. Sircar, J. Gliem and M. K. Chaudhury, *Langmuir*, 2004, **20**, 4085–4092.
22 S. Ghosh, P. Sharma and S. Bhattacharya, *Rev. Sci. Instrum.*, 2007, **78**, 115110.
23 S. Daniel, M. K. Chaudhury and P. G. DeGennes, *Langmuir*, 2005, **21**, 4240–4248.
24 J. M. Oh, S. H. Ko and K. H. Kang, *Langmuir*, 2008, **24**, 8379–8386.
25 K. R. Langley and J. S. Sharp, *Langmuir*, 2010, **26**(23), 18349–18356.
26 A. Shastry, M. J. Case and K. F. Bohringer, *Langmuir*, 2006, **22**, 6161–6167.
27 J. S. Sharp, D. J. Farmer and J. Kelly, *Langmuir*, 2011, **27**, 9367–9371.
28 M. A. Rodriguez-Valverde, F. J. Montes Ruiz-Cabello and M. A. Cabrerizo-Vilchez, *Adv. Colloid Interface Sci.*, 2008, **138**, 84–100.
29 C. S. Milner and N. N. Dalton (Ed.), *Glycerol*, Reinhold Publishing, New York, 1953.
30 M. L. Sheely, *Ind. Eng. Chem.*, 1932, **24**(9), 1060–1064.
31 J. B. Segur and H. E. Oberstar, *Ind. Eng. Chem.*, 1951, **43**(9), 2117–2120.
32 L. D. Landau and E. M. Lifshitz, *Fluid Mechanics*, 2nd Ed., Elsevier, Oxford, p245, 1987.
33 B. Christiansen, P. Alstrom and M. T. Levinsen, *J. Fluid Mech.*, 1995, **291**, 323–341.
34 J. Miles, *J. Fluid Mech.*, 1991, **222**, 197–205.
35 L. M. Hocking, *J. Fluid Mech.*, 1987, **179**, 253–266.
36 S. T. Milner, *J. Fluid Mech.*, 1991, **225**, 81–100.